ASSESSMENT OF TURBULENCE MODELLING FOR CFD SIMULATIONS INTO HYDROTURBINES: SPIRAL CASINGS

Luís C. Eduardo Oliveira de Souza, Marcelo Dias de Moura, Antonio C. P. Brasil Junior
Universidade de Brasília - Departamento de Engenharia Mecânica - Pós-Graduação
Laboratório de Energia e Ambiente - LEA
CEP 70.910-900 - Brasília - DF - Brasil
+55 (61) 307-2314 R236/238
duducastro@yahoo.com

Håkan Nilsson
Department of Thermo and Fluid Dynamics
Chalmers University of Technology
Göteborg, Sweden
hani@tfd.chalmers.se

Abstract. Spiral casings are applied to distribute the water, as evenly as possible, to the stay vanes and wicket gates and then to the turbine runner. In a well-designed spiral casing, the pressure head of the fluid should be made available to the runner with minimum loss, hence the analysis of the flow through a spiral casing is important for the design of efficient hydraulic turbines. The goal of this work is based on turbo machines spiral casings three-dimensional flow modeling, simulation and characterization. Governing equations related to their study are used in the mathematical modeling part. Therefore, several turbulence models available will be tested with a finite volume method based commercial software – CFX 5.5.1 which generates default tetrahedral meshing. Qualitative and quantitative results validation are proved by workshop benchmark experiments already done, in order these results can obtain a turbulence model that represents better the flow complexity inside spiral casings.

Keywords: Numerical simulation, spiral casings, CFD, Turbulence Models.

1. Introduction

Until a few years ago, hydromachines were built only using design methodologies based in empirical relations accumulated on two centuries of turbomachinery project experience. The enhancement of the hydroturbine efficiency on the last decade could only be reached by the use of modern design techniques based in Computational Fluid Dynamics (CFD). The progress of internal hidrodynamic design, using CFD, is a reality in modern hydroturbines projects, decreasing the time and costs for the project development. The use of CFD tools is an efficient and inexpensive way to make internal flow predictions accurately, and any sort of flow problems can be detected and further improvements can be made on the geometry component. Some articles have been published in the literature concerning the use of CFD as a tool of hydroturbine design (Maji and Biswas, 1998 and Maji and Biswas, 1999).

The commercial codes use a lot of alternatives for the modeling and simulation of internal flow problems. Many turbulence models could be used and different options of boundary conditions (wall laws, outflow, etc.) can be set. The assessment of turbulence modeling is a great contribution in order to verify the good alternatives of turbulence closure models, which reproduces a good agreement to the reality of the fluid flow. The main objective is to reproduce realistically the main structures of the three-dimensional fluid flow with a good estimative of pressure drop inside turbine components and torque on the runner surface. What kind of turbulence model works well to do this? Of course it is a difficulty problem because at each turbine component has specifically flow conditions which are much adaptable to a different alternative of turbulence model. The characteristic of the rotating flow through the runner and the flow inside the draft tube have important differences which are much treatable to some turbulence modeling strategies.

The aim of this paper is to evaluate three different models of turbulence (k-ε, k-ω and one equation model KE1E) for the use in the simulations of the spiral casing flows.

Usually in Kaplan or Francis turbines, spiral casings are employed to conduct water from the turbine entrance to the distributor. Built with complex geometry forms, a good spiral casing is projected to make sure that partial discharges pass through the guide vane inlet equally. To do this, its sections must gradually decrease towards the flow direction. Therefore, the main difficulties in a spiral casing project are to design such component to envoy fluid to the runner blades with minimum pressure head loss. Also, suggestions take as the generation of secondary flow what causes loss, Kurokawa and Nagahara (1986).

Flow analysis available in the open literature manipulates different methodologies for numerical simulation development. Maji and Biswas (1998) combined Petrov Galerkin finite element method to describe the flow structure in the spiral casing of a reaction turbine. L. Gros et all (1998), used the finite volume based commercial CFD code TASCflow and Nilsson and Davidson (2001), presented computational results with the finite volume CALC-PMB CFD code.

The simulation developed in the present paper is performed using the AEA Technology – CFX 5.5.1 commercial program. A spiral casing of Kaplan turbine model was used for present flow analysis. Three turbulence models – included on the code – have been tested to be compared with investigations already observed. Experimental results were performed by H. Nilsson et all (2001), on a project with the Swedish National Energy Administration and GE Energy (Sweden) AB, which supplied the geometry drawing and the measurements for comparison and code validation.

The hydraulic component was a Kaplan turbine semi-spiral casing. The investigated turbine consists of a 1:11 scale model of the Kaplan turbine. The model runner has a diameter D = 500mm, the runner speed N = 595 rpm and the volume flow Q = 0.522m³/s. Operating conditions for investigation is close to the best efficiency operating point, at 60% load.

On the present work, computation flow results must be indicated on the same location based on the experimental investigation, specifically, the region focused to observe flow in the distributor, where tangential and axial velocities are relevant.

Firstly, geometry has been redesigned on SolidWorks CAD software and inserted on CFD code as fluid domain, Fig. (1). Inlet and outlet boundary conditions are chosen following the three fluid turbulence models: (1) k-ε, (2) k-ω and (3) KE1E. (1) and (2) are two equations turbulence models and (3) is based on one equation model, Menter (1994).

Since in the open literature very few articles are available on computation analysis of this kind of geometry, this work aims to contribute to make CFD as a more popular tool among engineers because of its proposition of a good numerical solution that may sometimes replace older machine project methods.
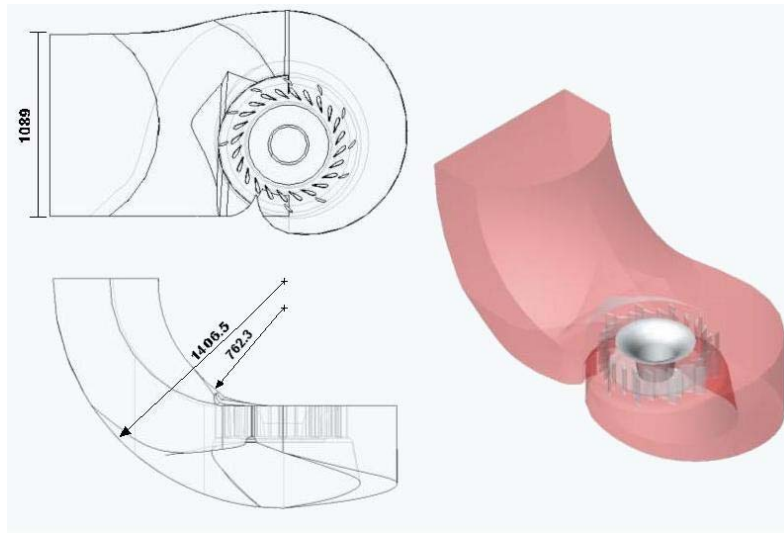

Figure 1. Spiral casing of the Kaplan turbine

2. Governing Equations

Flow is considered to be viscous, incompressible and turbulent. Domain is discretized into small tetrahedral volumes, as shown in Fig. (2) and special refinement around distributor surfaces, Fig. (3), were made for results precision. Momentum and mass conservation equations have been used here as governing equations. These equations can be written as the form shown bellow in Eq. (1) and Eq. (2) for mass and momentum conservation equations, respectively.

$$\nabla \vec{u} = 0 \tag{1}$$

$$\rho \frac{D\vec{u}}{Dt} = -\nabla p \vec{I} + \nabla \cdot \mathrm{T} \tag{2}$$

Where ρ is described as density, $\vec{u}$ is the velocity and its components are u, v and w for Cartesian directions x, y and z, respectively, p is taken as pressure, $\vec{I}$ is the identity tensor, T as the stress tensor, defined in Eq. (3) and $\rho D\underline{u}/Dt$ as the total derivative, as shown in Eq.(4). Equation (5) defines the strain tensor, $\underline{\underline{S}}$.

$$T = 2\mu\left[\underline{\underline{S}}(\vec{u}) - \frac{1}{3}tr(\nabla \cdot \vec{u})\right] \tag{3}$$

$$\rho \frac{D\vec{u}}{Dt} = \rho \frac{\partial \vec{u}}{\partial t} + \nabla \cdot (\rho \vec{u} \otimes \vec{u}) \tag{4}$$

$$\underline{\underline{S}}(\vec{u}) = \frac{1}{2}\left[\nabla\vec{u} + \nabla^T\vec{u}\right]$$ (5)
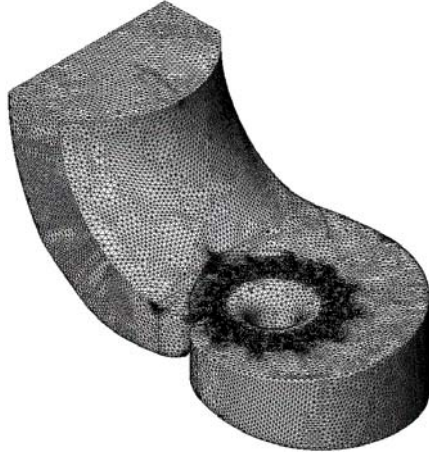

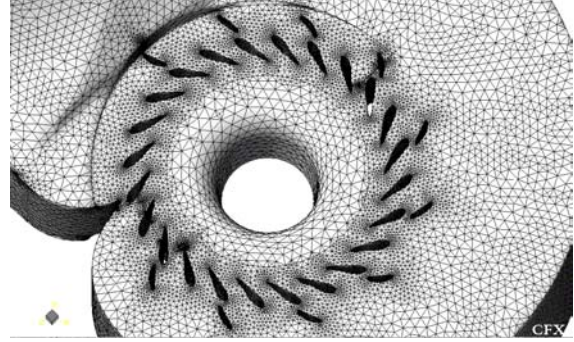Figure 2. Spiral casing tetrahedral meshing.

Figure 3. Meshing refinement around stay and guide vanes.

General governing equations are used for a basic knowledge of the code. Besides, some restrictions were considered for computational cost proposes, such as consider fluid flow incompressible and permanent.
Turbulence models used by CFX 5.5.1 are showed in the section below, AEA Technology (2002).

2.1. Turbulence Models

2.1.1 The k – ε model

The k-ε (k-epsilon) model is the industry standard two-equation turbulence model. k is the turbulence kinetic energy and is defined as the variance of the fluctuations in velocity. It has dimensions of ($L^2 T^{-2}$), e.g. m²/s². e is the turbulence eddy dissipation (the rate at which the velocity fluctuations dissipate) and has dimensions of k per unit time ($L^2 T^{-3}$), e.g. m²/s³.

The k-e model, like the zero equation model, is based on the eddy viscosity concept, so that in Eq. (6).

$$\mu_{ef} = \mu + \mu_t$$ (6)

where μ_{ef} is the effective viscosity accounting for turbulence, μ_t is the turbulent viscosity. The k-ε model assumes that the turbulence viscosity is linked to the turbulence kinetic energy and dissipation via the relation in Eq. (7).

$$\mu_t = c_\mu \rho \frac{k^2}{\varepsilon}$$ (7)

where c_μ is a constant with and its value is 0.09. The values of k and ε come directly from the differential transport equations for the turbulence kinetic energy and turbulence dissipation rate as shown in Eq. (8) and Eq. (9), respectively.

$$\frac{\partial\rho k}{\partial t} + \nabla\cdot\left(\rho\vec{U}k\right) - \nabla\cdot\left(\frac{\mu_{ef}}{\sigma_k}\nabla k\right) = P_k - \rho\varepsilon$$ (8)

$$\frac{\partial\rho\varepsilon}{\partial t} + \nabla\cdot\left(\rho\vec{U}\varepsilon\right) - \nabla\cdot\left(\frac{\mu_{ef}}{\sigma_\varepsilon}\nabla\varepsilon\right) = \frac{\varepsilon}{k}\left(c_{\varepsilon 1}P_k - c_{\varepsilon 2}\rho_\varepsilon\right)$$ (9)

where the constants $c_{\varepsilon 1} = 1.44$, $c_{\varepsilon 2} = 1.92$, $\sigma_k = 1$ e $\sigma_\varepsilon = 1.3$. P_k is the shear production due to turbulence, which for incompressible flows is as Eq. (10).

$$P_k = \mu_t\nabla\vec{U}\cdot\left(\nabla\vec{U} + \nabla\vec{U}^T\right) - \frac{2}{3}\nabla\cdot\vec{U}\left(\mu_t\nabla\cdot\vec{U} + \rho k\right)$$ (10)

2.1.2. The k – ω model

One of the advantages of the *k-ω* formulation is the near wall treatment for low-Reynolds number computations. The model does not involve the complex non-linear damping functions required for the *k-ε* model and is therefore more accurate and more robust. A low-Reynolds number grid would require a near wall grid resolution of at least $y^+ < 2$.

This condition cannot be guaranteed in most applications and for this reason, a new near wall treatment was developed for the *k-ω* model. It allows for smooth shift from a low-Reynolds number form to a wall function formulation.

The starting point of the present formulation is the *k-ω* model developed by Wilcox (1986). It solves two transport equations, one for the turbulent kinetic energy, *k*, and one for the turbulent frequency, ω, respectively for Eq. (11) and Eq. (12). The stress tensor is computed from the eddy-viscosity concept.

$$\frac{\partial \rho k}{\partial t} + \nabla \cdot \left(\rho \vec{U} k \right) = P_k - \beta' \rho k \omega + \nabla \cdot \left(\mu + \frac{\mu_t}{\sigma_k} \nabla k \right) \tag{11}$$

$$\frac{\partial \rho \omega}{\partial t} + \nabla \cdot \left(\rho \vec{U} \omega \right) = \alpha \frac{\omega}{k} P_k - \beta \rho \omega^2 + \nabla \cdot \left[\left(\mu + \frac{\mu_t}{\sigma_\omega} \right) \nabla \omega \right] \tag{12}$$

In addition to the independent variables, the density, ρ, and the velocity vector, $\vec{U}$, are treated as known quantities from the Navier-Stokes method. In Equation (13), P_k is the production rate of turbulence with the strain tensor $\underline{\underline{S}}$, as shown in Eq. (5).

$$P_k = \mu_t 2 \underline{\underline{S}} : \nabla \vec{U} \tag{13}$$

constants are given by $\beta' = 0.09 \quad \alpha = \frac{5}{9} \quad \beta = \frac{3}{40} \quad \sigma_k = 2 \quad \sigma_\omega = 2$

and the unknown Reynolds stress tensor, $\vec{\tau}$, is calculated from Eq. (14).

$$\vec{\tau} = \mu_t 2 \underline{\underline{S}} - \rho \frac{2}{3} \delta k \tag{14}$$

2.1.3. The one equation model – KE1E

This one equation model was developed by Menter (1994) which allows a transformation of the two equation turbulent viscosity models into one equation turbulence model. Menter followed Baldwin & Barth (1990) to describe one equation models and expressed the time derivative of the eddy viscosity by the times derivatives of k and ε, as shown in Eq. (15).

$$\frac{D \widetilde{v}_t}{Dt} = c_\mu \left(2 \frac{k}{\varepsilon} \frac{Dk}{Dt} - \frac{k^2}{\varepsilon^2} \frac{D\varepsilon}{Dt} \right) \tag{15}$$

Equation (16) refers to the definition of the eddy viscosity:

$$\widetilde{v}_t = c_\mu \frac{k^2}{\varepsilon} \tag{16}$$

and a single transport equation for the eddy viscosity, which, however, depends on k and ε as well as on the eddy viscosity was found in Eq. (17).

$$\frac{D \widetilde{v}_t}{Dt} = f(\widetilde{v}_t, k, \varepsilon) \tag{17}$$

Since a complete set of equations, the one equation model can be derived by straightforward substitution, as shown in Eq. (18).

$$\frac{D \widetilde{v}_t}{Dt} = c_1 D_1 \widetilde{v}_t \Omega - c_2 E_{1e} + \nabla \left[\left(v + \frac{\widetilde{v}_t}{\sigma} \right) \nabla (\widetilde{v}_t) \right] \tag{18}$$

Ω is the absolute vorticity and the constants of the model indicate the following values:

$$c_1 = (c_{\varepsilon 2} - c_{\varepsilon 1})c_\mu^{1/2} = 0.144 \qquad \sigma = \sigma_k = 1 \qquad c_2 = c_1 \kappa^{-2} + \sigma^{-1} = 1.86 \qquad \kappa = 0.41$$

$$D_1 = \frac{v_t + v}{\tilde{v}_t + v} \qquad D_2 = 1 - e^{-\left(\frac{\tilde{v}_t}{A^+ \kappa v}\right)} \qquad A^+ = 13.5$$

where $c_{\varepsilon 2}$, $c_{\varepsilon 1}$ and c_μ are the same values showed in the k-ε model definition.

3. Flow survey and simulation

The following sections refer to the simulations done with the three turbulence models including experimental results. Since experimental investigation consists of LDV (Laser Doppler Velocimetry) measurements, a comparison with the simulations in the same section has been decided. Figure (4) shows the plane used for measurements as well as for the simulation. Quantitative results were performed in a plot of velocities near the bend region in front of guide vanes. Figure (5) shows the velocity profile on the bend region. Results are available in mean tangential velocity and mean axial velocity.

LDV measurements are based in two components. Tangential velocity is normal to the measurement plane and the axial velocity denotes the vertical velocity.

To observe the same velocities in the plane on the simulation, some equation expressions have been inserted into the post-processing software to calculate each component.
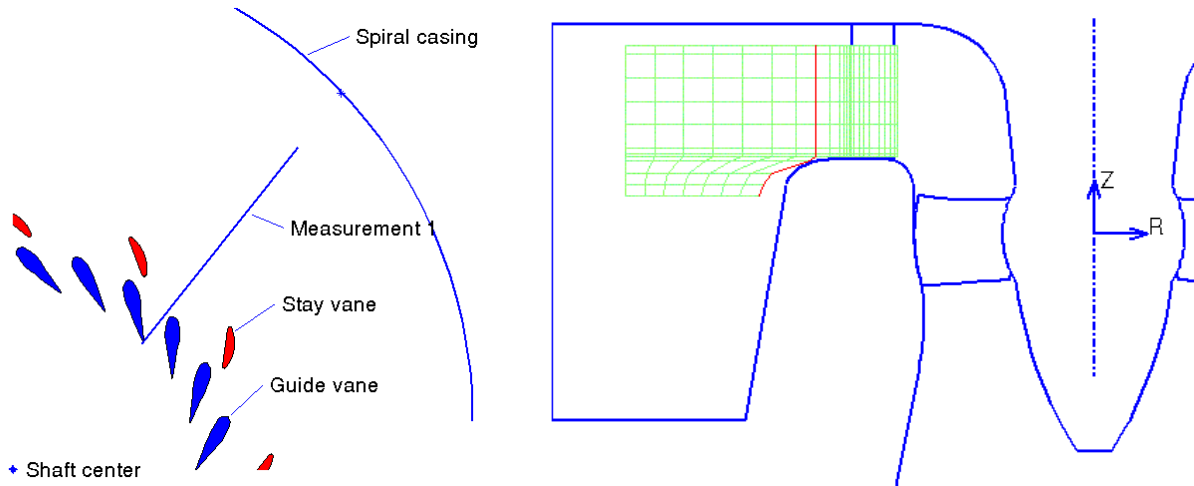

Figure 4. Top view of the direction of the measurement.   Figure 5. Velocity profile at the bend region.

The experimental investigation used LDV measurements for validation of computations of the flow in the distributor. The LDV technique uses the Doppler shift of reflected light particles and translates instantaneous velocity in a single point. Because of the characteristics of this kind of measurements, the laser beam needs transparent wall and fluid to work correctly. Thus, a number of plexiglass windows have been installed in the water turbine model. Because of some difficulties to position the laser beam to get measurements, it was necessary to do them through the side of the spiral casing slightly non-orthogonal to the window (10.8°). By doing this, it was capable of making measurements as far as possible into the distributor and avoids reflections from a guide vane. Additional description of the LDV technique is presented by Andersson (2000).
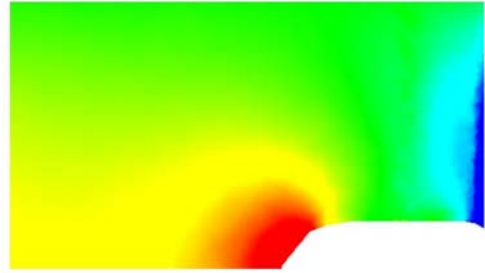
3.1. Results and discussion

The CFD code allows the insertion of additional information about restrictions to be made. Initial and boundary conditions for velocities are inserted as following:

- Inlet: $\dot{m}$ = mass flow = 522 kg/s at the intake;

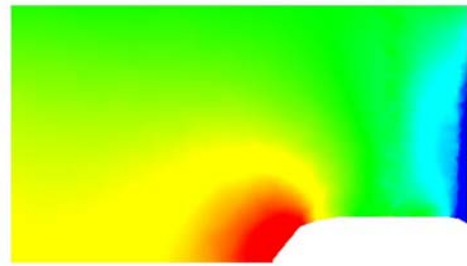- Outlet: p = relative pressure with respect with local ambient = 0 at the exit boundary.

Figure 6. a- Mean tangential velocity – k-ε (m/s)   b- Mean axial velocity – k-ε (m/s)
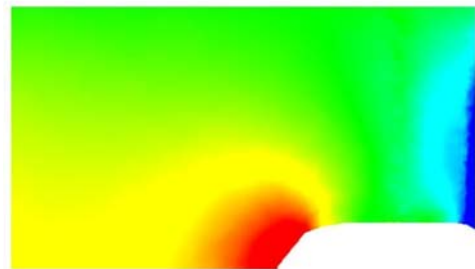

Figure 7. a- Mean tangential velocity – k-ω (m/s)   b- Mean axial velocity – k-ω (m/s)

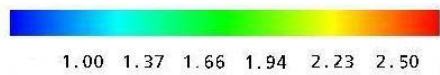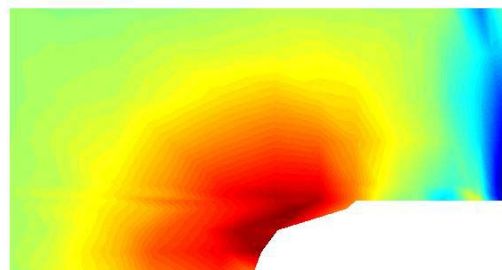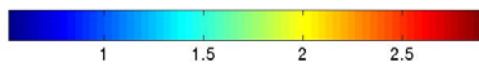Figure 8. a- Mean tangential velocity – KE1E (m/s)   b- Mean axial velocity – KE1E (m/s)

1.00   1.37   1.66   1.94   2.23   2.50   -0.60 -0.43 -0.26 -0.09 0.09 0.26 0.43 0.60

Figure 9. a- Mean tangential velocity – experimental (m/s)   b- Mean axial velocity – experimental (m/s)

1   1.5   2   2.5   -0.6   -0.4   -0.2   0   0.2   0.4   0.6
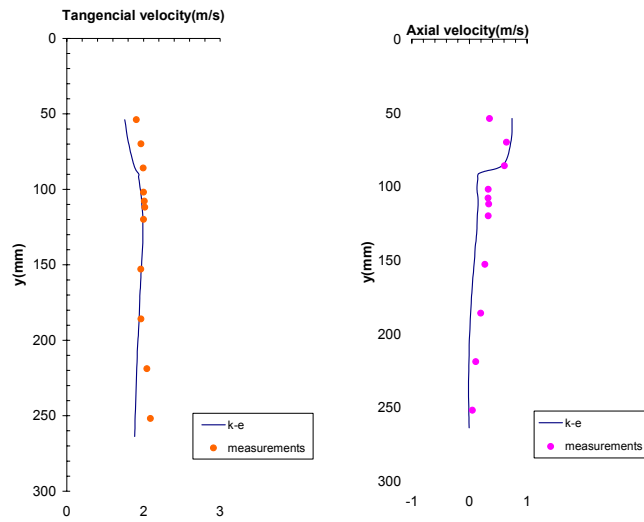
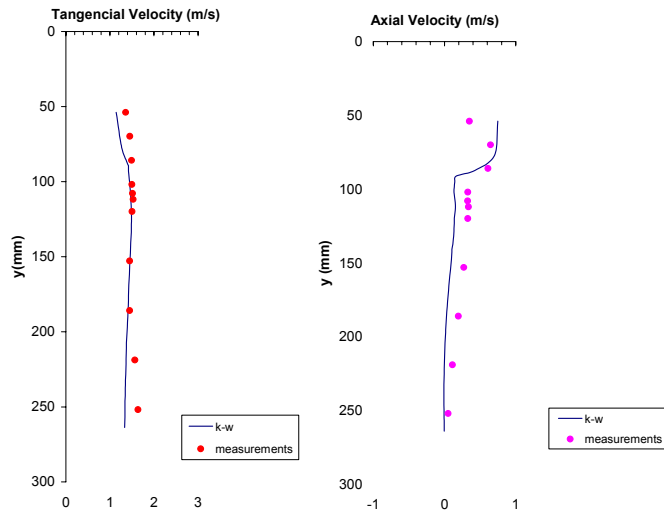Figure 10. k-ε model and experimental results – velocity profile.

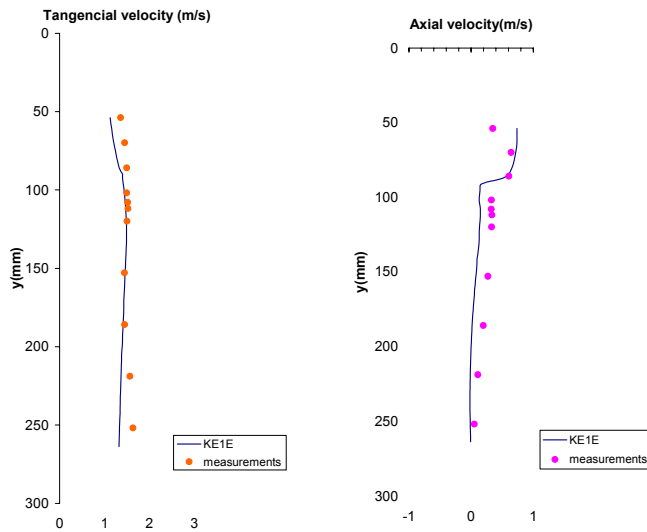Figure 11. k-ω and experimental results – velocity profile.

Figure 12. KE1E - one equation model and experimental results – velocity profile.

In the spiral casing, tree-dimensional tetrahedral meshing has been formed. Meshing generation can be described as the whole fluid domain and the distributor components as no slip wall condition. In order to determine a steady state value, a 10^{-5} convergence criterion has been chosen with predefined timescale control for each turbulence model (484096 nodes and 2621366 elements). For k-ε and k-ω models, CPU time required to solve the numerical problem was about 3 hours and for the one equation model (KE1E), about 2 hours on a 2GB RAM, 2.0 GHz Pentium 4 Dell 340 Precision. See table 1 for CPU time detailed information.

Table 1. Turbulence models outer loop iteration numbers and convergence CPU time.

Turbulence Model	Number of Iterations	CPU time (s)
k-ε	41	11242.87
k-ω	41	11220.75
KE1E	18	7049.51

Simulation shows contour of the tangential velocity in the local measurement plane, for the three turbulence models in Fig. (6.a), Fig. (7.a) and Fig. (8.a) had almost same gradient velocity behavior. A velocity increase at the lower ring due to the smaller area at the distributor region has been detected. Also a stagnation region is located at the front of the guide vanes. In experimental measurements, according to H. Nilsson et all (2001), the main features of the flow in the distributor are that the tangential velocity component increases at the lower ring, as shown in Fig. (9.a), which is an effect of the sharp bend of the flow after the distributor. A stagnation region occurs in front of a guide vane, a guide vane wake region is present at the radially innermost of the measurements and there is a sharp increase in the magnitude of the axial velocity component close to the bend of the flow, as seen on Fig. (9.b).

In both type of results, simulation and experimental measurements, similar velocity contours can be seen. At the outer region of the spiral casing, flow seems to be slightly slower than experimental results. Simulation detects tangential velocity increase also from the top of the spiral casing to the outlet region.

Figure (6.b), Fig. (7.b) and Fig. (8.b) show mean axial velocity contour at the same measurement plane. A velocity increase is detected at the bend region. It decreases at the guide vane entrance and at the inner section of the plane, velocity suddenly increases due to the runner entrance. Simulations agree with experimental results concerning to the velocity increase at the bend region and flow behavior.

Figure (10), Fig. (11) and Fig. (12) plot the tangential and axial velocities distributions in a profile at the bend region, as seen on the highlighted red line in Fig. (5). Results show good agreement with those presented by H. Nilsson et all (2001) measurements.

Figure (15) shows streamline velocity from the intake to the spiral casing exit. Flow structure is almost radial at the exit region (after the stay and guide vanes region). Figure (13) shows velocity vectors at a horizontal mid-plane. Figure (14) shows vectors closely at the guide vane passage. Fluid contours the vane surface avoiding recirculation from the distributor entrance and rotating flow for runner at the outlet region is distributed circumferentially. Finally, Fig. (16) shows axial at the spiral casing outlet. Velocity is almost well distributed considering variation around the component wall.

Concerning computing cost and time considerations, the one equation model solved successfully the simulation showing similar results and it was calculated in a few numbers of iterations for convergence comparing the two other models.
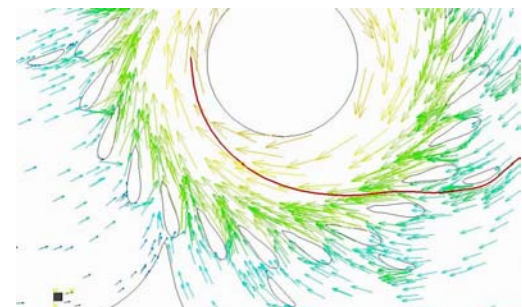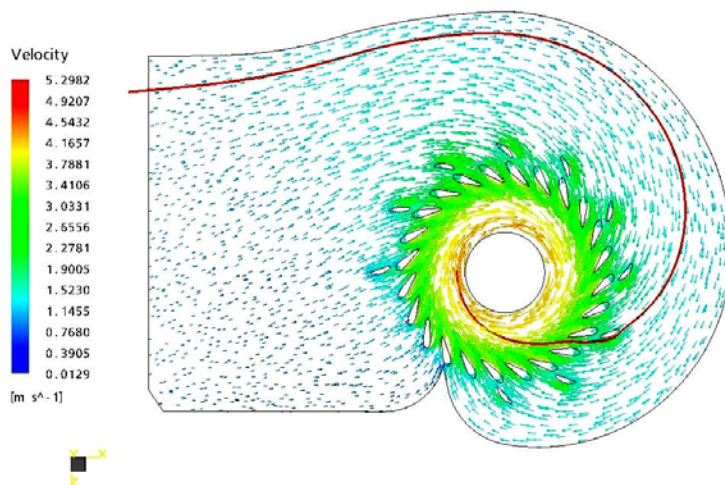

Figure 13. Velocity vectors projection at the horizontal mid-plane.   Figure 14. A closer look at the velocity vectors
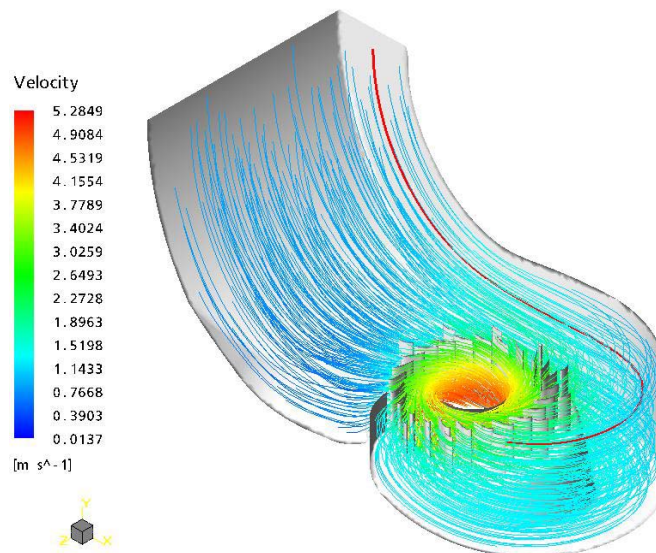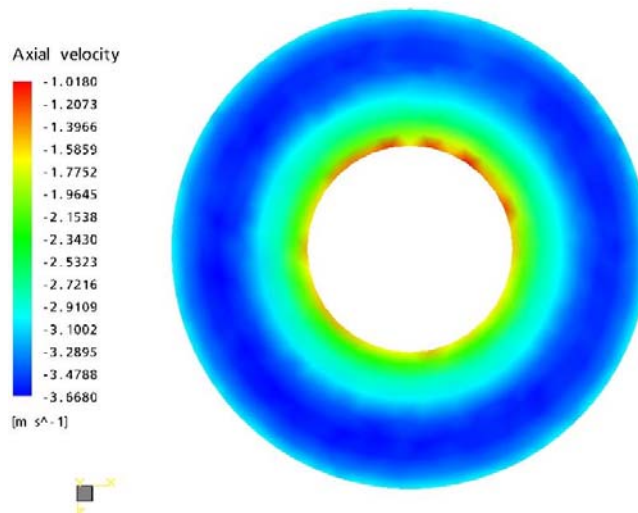
Figure 15. Plot of streamline velocity

Figure 16. Axial velocity at the spiral casing outlet.

4. Conclusions

The flow structure simulation using three different turbulence models to compare with experimental results have been obtained using a finite volume based CFD tool with tetrahedral meshing generated for analysis. Results show good qualitative and quantitative agreement with measurements and all the models successfully analyzed the three-dimensional flow at an extremely complex geometry hydro machine component at the same experimental operating condition. The CFD code contributes to develop design efficiently hydraulic turbines which are a field that lacks hydrodynamics theory application.

5. References

AEA Technology, 2002, "Introduction to CFX 5 version 5.5.1", United Kingdom, 276 p.

Andersson, U. and Karlsson, R., 2000, "Quality aspects of the Turbine 99 draft tube experiment". Proceedings from Turbine 99 – workshop on draft tube flow, ISSN: 1402-1536.

Gros, L., Kueny, J.L., Avellan, F. and Bellet, L., 1998, "Numerical flow analysis of the GAMM turbine at nominal and off-design operating conditions", Proceedings of the XIX IAHR Symposium, Hydraulic Machinery and Cavitation, pp.121-128.

Kurokawa, J. and Nagahara, H., 1986, "Flow characteristics in spiral casings in water turbines", IAHR Symp., Montreal, Canada, Vol. 2, Paper No. 62.

Maji, P.K. and Biswas, G., 1998, "Three-dimensional analysis of flow in the spiral casing of a reaction turbine using a differently weighted Petrov Galerkin method", Computer Methods in Applied Mechanics and Engineering, Vol. 167, pp. 167-190.

Maji, P.K. and Biswas, G., 1999, "Analysis of flow in the spiral casing using a streamline upwind Petrov Galerkin method", International Journal for Numerical Methods in Engineering, Vol. 45, pp. 147-174.

Menter, F.R., 1994, "Eddy Viscosity Transport Equations and their Relation to the k-ε Model", ASME Journal of Fluids Engineering, Vol. 119, pp. 876-884.

Nilsson, H., Andersson, U. and Videhult, S., 2001, "An experimental investigation of the flow in the spiral casing and distributor of the Hölleforsen Kaplan turbine model", Publication 01/05, Chalmers University of Technology, Göteborg, Sweden, 12 p.

Nilsson, H. and Davidson, L., 2001, "A validation of parallel multiblock CFD against the GAMM Francis water turbine runner at best efficiency and off-design operating conditions", Publication 02/05, Chalmers University of Technology, Göteborg, Sweden, 42 p.